Anillin promotes astral microtubule-directed cortical myosin polarization

Yu Chung Tse[a], Alisa Piekny[b], and Michael Glotzer[a]
[a]Department of Molecular Genetics and Cell Biology, University of Chicago, Chicago, IL 60637; [b]Department of Biology, Concordia University, Montreal, Quebec H4B 1R6, Canada

ABSTRACT **Assembly of a cytokinetic contractile ring is a form of cell polarization in which the equatorial cell cortex becomes differentiated from the polar regions. Microtubules direct cytokinetic polarization via the central spindle and astral microtubules. The mechanism of central spindle–directed furrow formation is reasonably well understood, but the aster-directed pathway is not. In aster-directed furrowing, cytoskeletal factors accumulate to high levels at sites distal to the asters and at reduced levels at cortical sites near the asters. In this paper, we demonstrate that the cytoskeletal organizing protein anillin (ANI-1) promotes the formation of an aster-directed furrow in *Caenorhabditis elegans* embryos. Microtubule-directed nonmuscle myosin II polarization is aberrant in embryos depleted of ANI-1. In contrast, microtubule-directed polarized ANI-1 localization is largely unaffected by myosin II depletion. Consistent with a role in the induction of cortical asymmetry, ANI-1 also contributes to the polarization of arrested oocytes. Anillin has an evolutionarily conserved capacity to associate with microtubules, possibly providing an inhibitory mechanism to promote polarization of the cell cortex.**

Monitoring Editor
David G. Drubin
University of California, Berkeley

Received: May 5, 2011
Revised: Jun 27, 2011
Accepted: Jun 28, 2011

INTRODUCTION

Cytokinesis, the creation of two daughter cells from a single parental cell, is driven by the constriction of an actomyosin-based contractile ring juxtaposed to the plasma membrane. The ring defines a plane that lies perpendicular to the anaphase spindle. Assembly and constriction of the contractile ring at the correct time and place are essential for the generation of viable daughter cells. Contractile ring formation requires local activation of the small GTPase RhoA, which promotes actin polymerization and activation of nonmuscle myosin (reviewed in Piekny *et al.*, 2005; Bement *et al.*, 2006). The motor activity of nonmuscle myosin slides actin filaments, thereby generating the force that drives membrane ingression. Once the furrow ingresses extensively, a structure termed the midbody is formed, which stabilizes the ingressed furrow until the membrane undergoes abscission.

The position of the contractile ring is determined by the mitotic spindle during anaphase. Two features of the spindle control furrow positioning: the central spindle and astral microtubules (reviewed in D'Avino *et al.*, 2005; von Dassow *et al.*, 2009). The central spindle is composed of antiparallel microtubule bundles that lie between the segregating chromosomes during anaphase, while astral microtubules emanate radially from centrosomes at the two spindle poles (reviewed in Glotzer, 2009). Although the central spindle is required for completion of cytokinesis, cells with compromised central spindles still form ingressing cleavage furrows at a site dictated by the asters (Dechant and Glotzer, 2003). The two mechanisms for furrow induction have been extensively studied using *Caenorhabditis elegans* embryos (Dechant and Glotzer, 2003; Bringmann and Hyman, 2005; Werner *et al.*, 2007; Lewellyn *et al.*, 2010). However, there is compelling evidence that both pathways contribute to cytokinesis in a variety of metazoan cells (Alsop and Zhang, 2003; Murthy and Wadsworth, 2008; Piekny and Glotzer, 2008; von Dassow *et al.*, 2009). Although these two mechanisms for furrow induction can function independently, they cooperate to result in more rapid induction of furrows (Dechant and Glotzer, 2003). The astral microtubule-directed pathway may play

This article was published online ahead of print in MBoC in Press (http://www.molbiolcell.org/cgi/doi/10.1091/mbc.E11-05-0399) on July 7, 2011.

Address correspondence to: Michael Glotzer (mglotzer@uchicago.edu).

Abbreviations used: AP, anterior–posterior; APC, anaphase-promoting complex; DTT, dithiothreitol; EGTA, ethylene glycol tetraacetic acid; HIS, histone; IPTG, isopropyl β-D-1-thiogalactopyranoside; NCRR, National Center for Research Resources; NGM, nematode growth medium; NIH, National Institutes of Health; PBS, phosphate-buffered saline; PBST, phosphate-buffered saline Tween-20; PH, pleckstrin homology; RhoGAP, Rho family GTPase-activating protein; RhoGEF, Rho family guanine nucleotide exchange factor; RNAi, RNA interference; STC, *S*-trityl-L-cysteine.

a particularly important role in large cells in which the central spindle is distant from the cell cortex.

The central spindle and astral arrays direct cleavage furrow formation via distinct molecular mechanisms. Central spindle microtubules are bundled by centralspindlin (a complex consisting of the GTPase-activating protein [RhoGAP] CYK-4/MgcRacGAP and the kinesin-6 motor protein ZEN-4/MKLP1), as well as other microtubule-associated proteins (Glotzer, 2009). During anaphase, a Rho guanine nucleotide exchange factor (RhoGEF), Ect2, localizes to the antiparallel microtubules in the spindle midzone by binding to Plk1-phosphorylated HsCYK4 (Burkard *et al.*, 2009; Wolfe *et al.*, 2009). This interaction appears essential for activation of the exchange function of Ect2, as RhoA activation is abrogated in cells in which the interaction is prevented (Burkard *et al.*, 2007; Petronczki *et al.*, 2007).

When central spindle assembly is impaired, and asters direct furrow formation, RhoA is globally activated in an Ect2-dependent manner leading to the global cortical recruitment of RhoA effectors (Werner *et al.*, 2007). The accumulation of these effectors is modulated by an inhibitory cue from astral microtubules, a process known as astral relaxation. Specifically, in *C. elegans* embryos, a posteriorly positioned spindle locally inhibits myosin accumulation in the posterior, with the exception of a small amount of myosin that accumulates directly over the central spindle, leading to furrow formation in both the anterior and posterior (Werner *et al.*, 2007). Therefore, cleavage furrow formation is mediated by a combination of two mechanistically distinct pathways. However, the molecular mechanism by which cortical myosin recruitment is spatially regulated by astral microtubules is not yet known.

There are notable similarities between the aster-directed furrow and the pseudocleavage furrow that accompanies embryo polarization. *C. elegans* zygotes are not initially polarized. Sperm entry and migration of the sperm pronucleus and its associated centrosome to the nearest pole establishes the posterior (St Johnston and Ahringer, 2010). The sperm-derived centrosome is essential for polarity determination, and causes a local cessation of a cortical contractility (Cowan and Hyman, 2004). This symmetry-breaking event triggers a contractile wave that results in the anterior enrichment of the initially ubiquitous anterior PAR complex and the posterior cortical accumulation of the posterior PAR complex (Munro *et al.*, 2004). During this initial polarization stage, a pseudocleavage furrow ingresses at the anterior–posterior (AP) boundary. The genetic requirements of pseudocleavage and aster-directed furrowing overlap extensively (Werner and Glotzer, 2008; Schenk *et al.*, 2010), suggesting similar underlying molecular mechanisms.

We sought to determine the molecular mechanism by which microtubules locally modulate cortical myosin accumulation. Previous studies have revealed that, whereas small foci of cortical myosin accumulate in the vicinity of the astral arrays, large myosin foci only form at sites of low microtubule density (Werner *et al.*, 2007). Because anillin colocalizes with and mediates the formation of large myosin foci prior to pronuclear migration and cytokinesis in *C. elegans* embryos (Maddox *et al.*, 2005; Werner and Glotzer, 2008), we investigated whether anillin contributes to astral relaxation.

Anillin is a multifunctional protein that becomes highly concentrated in the contractile ring (see Piekny and Maddox, 2010, for review). Anillin organizes the cortical cytoskeleton via interactions with F-actin, myosin, RhoA, septins, and formin, and therefore acts as a cytoskeletal scaffold protein (Field and Alberts, 1995; Straight *et al.*, 2005; Piekny and Glotzer, 2008; Watanabe *et al.*, 2010). The *C. elegans* genome encodes three isoforms of anillin, ANI-1, ANI-2, and ANI-3 (Maddox *et al.*, 2005). Whereas ANI-3 has no known function and ANI-2 contributes to the organization of the gonad, ANI-1 contributes to the organization of the cortical cytoskeleton during polarization and cytokinesis (Maddox *et al.*, 2005). ANI-2 is present in embryos, but it only subtly modulates cortical contractility due to its inhibition by PAR-4/LKB1 (Chartier *et al.*, 2011). Although ANI-1–depleted *C. elegans* embryos complete cytokinesis, the cytokinetic furrows ingress symmetrically, whereas the furrows in control embryos are asymmetric (Maddox *et al.*, 2007). ANI-1 is also essential for furrowing in embryos with compromised central spindles (Werner and Glotzer, 2008). Collectively, these data suggest that anillin regulates aster-directed furrow formation; however, the underlying mechanism remains to be determined.

RESULTS

Anillin mediates aster-mediated furrowing

Previous analysis indicated ANI-1 primarily contributes to the central spindle–independent pathway for furrow ingression in *C. elegans* embryos (Werner and Glotzer, 2008). To confirm and extend these results, we examined the contribution of anillin to the ingression of anterior and posterior furrows in *zyg-9(b244ts)* embryos. ZYG-9 is a crucial microtubule-associated protein responsible for rapid microtubule growth (Matthews *et al.*, 1998; Srayko *et al.*, 2005). Inactivation of ZYG-9 permits spatial separation of the central spindle–dependent and aster-dependent furrows in the posterior and the anterior of the *C. elegans* zygote, respectively (Figure 1A; Werner *et al.*, 2007). The midzone of the posterior spindle locally induces formation of the central spindle–directed furrow, and the spindle

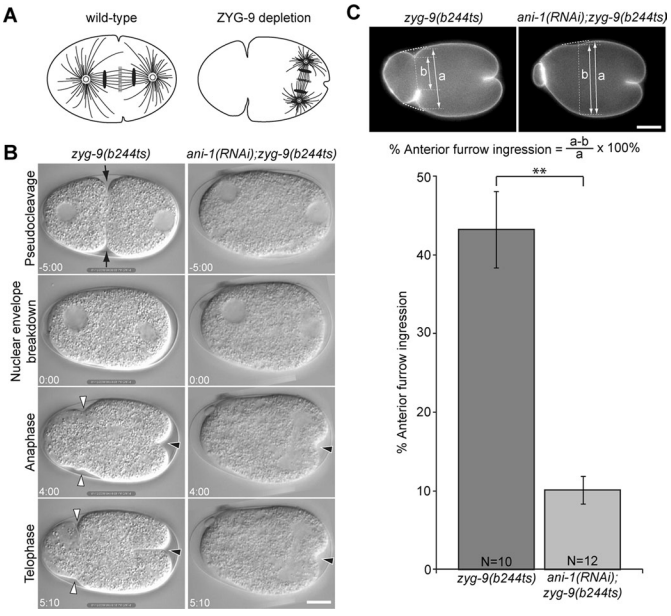

FIGURE 1: Anillin is required for aster-mediated furrow ingression. (A) Schematic depicting the position of the spindle in a wild-type embryo and a ZYG-9–depleted embryo with reduced aster size. (B) Images from a time-lapse sequences of the first division of *zyg-9(b244ts)* and *ani-1(RNAi);zyg-9(b244ts)* embryos. *zyg-9(b244ts)* mutant embryos form pseudocleavage furrows (black arrows) and anterior (white arrowheads) and posterior (black arrowheads) furrows during anaphase, whereas *ani-1(RNAi);zyg-9(b244ts)* embryos only form posterior furrows (black arrowheads) during anaphase. (C) The maximal extent of anterior furrow formation was quantitated using GFP::PH as a membrane marker as diagrammed. Error bars in the bar chart represent ± SEM. **, $p < 0.01$. All images are arranged with anterior to the left. Scale bars: 10 μm.

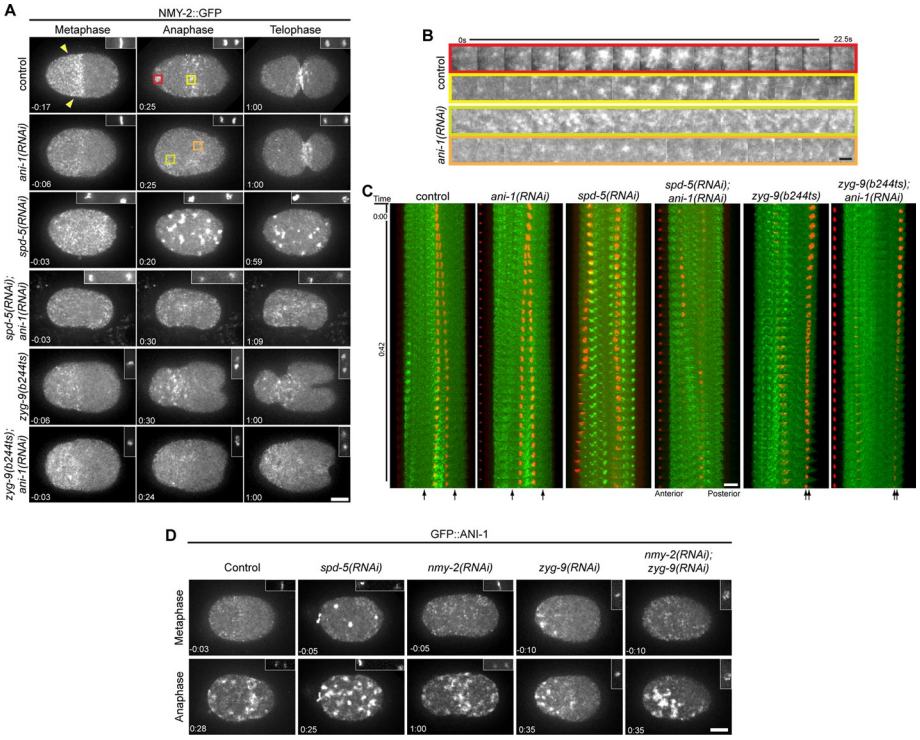

FIGURE 2: Microtubules control the distribution of cortical myosin. (A) Selected images from time-lapse sequences of embryos expressing NMY-2::GFP at the indicated cell cycle phases. Myosin images are maximum-intensity projections of five planes spanning 2 µm. Time relative to anaphase onset is shown, and the insets in the upper right of each frame show the chromatin imaged with GFP::HIS. (B) Detailed view of the behavior of representative foci (represented by the color coding in A) in control and *ani-1(RNAi)* embryos. (C) Kymograph analysis of the first 42 s after anaphase onset demonstrating the relative position of the myosin foci (green) and the chromatin (red). The approximate positions of the centrosomes, inferred by the position of the chromatin, are indicated by arrows at the bottom. (D) Selected images from time-lapse sequences of embryos expressing GFP::ANI-1 at the indicated cell cycle phases. The insets in the upper right of each frame show the chromatin imaged with mCherry::HIS. Scale bars: 10 µm (A, C, and D); 2 µm (B).

asters induce an anterior-biased accumulation of myosin, triggering ingression of a furrow in the anterior of the embryo. To facilitate measurement of the extent of membrane ingression, we labeled the plasma membrane with green fluorescent protein–pleckstrin homology (GFP::PH from PLC∂1; Audhya *et* al., 2005). On fertilization of *zyg-9(b244ts)* embryos at nonpermissive temperature (25°C), migration of the female pronucleus toward the male pronucleus failed, and the female and male pronuclei remained in the anterior and posterior poles, respectively (Figure 1B, Supplemental Fig1Video1). After nuclear envelope breakdown, the posterior-localized centrosomes directed spindle assembly around the male pronucleus. On anaphase onset, two independent furrows formed in the anterior and posterior (Figure 1B and Supplemental Fig1Video1). We measured the extent of membrane ingression during anaphase and found that anterior furrows ingressed to ~40% of the embryo width in *zyg-9(b244ts)* embryos (n = 10). In sharp contrast, in *ani-1(RNAi);zyg-9(b244ts)* embryos, anterior furrows only ingressed to an average of 10% of the embryo width (Figure 1, B and C, and Supplemental Fig1Video1; n = 12). Twenty-five percent of embryos lacked anterior furrows altogether. Posterior furrows ingressed to at least 35% of egg length, irrespective of ANI-1 depletion. In addition, we observed that pseudocleavage was abolished in both *ani-1(RNAi)* and *ani-1(RNAi);zyg-9(b244ts)* embryos, indicating effective depletion of ANI-1 (Figure 1B). These results suggest that anillin primarily contributes to induction of the anterior furrow.

Microtubules inhibit myosin recruitment in an anillin-dependent manner

To investigate how anillin regulates anterior furrow formation, we examined cortical myosin dynamics during the first cell division. GFP-tagged nonmuscle myosin II (NMY-2::GFP) and histone H2B (GFP::HIS) were coexpressed and visualized sequentially at different focal planes to correlate cortical events with cell cycle progression. As reported previously, prior to metaphase, small NMY-2::GFP puncta are enriched in the anterior half of the embryos, forming a dense anterior cap (Figure 2A, arrowheads; Munro *et al.*, 2004; Werner *et al.*, 2007). On anaphase onset, the anterior cap dissipated and a morphologically distinct set of NMY-2::GFP foci accumulated and coalesced to form large foci in the equatorial region and near the anterior pole (Figure 2, A–C, and Supplemental Fig2Video1). High-magnification views of myosin foci in both regions revealed that small, dim foci progressively intensified over a period of ~10 s and subsequently faded with similar kinetics (Figure 2B). In addition, neighboring foci coalesced to a single bright spot as judged by light microscopy. In contrast, in *ani-1(RNAi)* embryos, although NMY-2::GFP foci accumulated in the cell cortex, they failed to coalesce (Figure 2, A–C and Supplemental Fig2Video1).

Next we examined myosin recruitment in embryos devoid of organized arrays of microtubules as a consequence of depletion of the pericentrosomal component SPD-5 (Hamill *et al.*, 2002). In SPD-5–depleted embryos undergoing anaphase, large, bright NMY-2::GFP foci accumulated throughout the entire cell cortex (Figure 2, A and C, and Supplemental Fig2Video1). Formation of these large foci is dependent on anillin, as they are absent from the entire cortex of *spd-5(RNAi);ani-1(RNAi)* embryos. In these embryos myosin accumulated in small foci throughout the cortex (Figure 2, A and C, and Supplemental Fig2Video1). We infer that anillin has the potential to promote myosin coalescence globally, and that its activity is modulated by microtubules.

To further establish that microtubules regulate cortical myosin accumulation, we generated microtubule-depleted and microtubule-dense regions in the same embryo by depleting ZYG-9 (Figures 1A and 2, A and C). During anaphase, large cortical NMY-2::GFP foci were only observed in the anterior half of ZYG-9–depleted embryos; the small foci that accumulated in the vicinity of the posterior spindle failed to coalesce, except immediately adjacent to the central spindle (Figure 2, A and C, and Supplemental Fig2Video1). Kymographic analysis revealed that large, intense myosin foci accumulated at sites distal to the spindle poles when ANI-1 was present (Figure 2C).

To determine whether the inverse correlation between microtubule-dense regions and myosin coalescence is anillin-dependent,

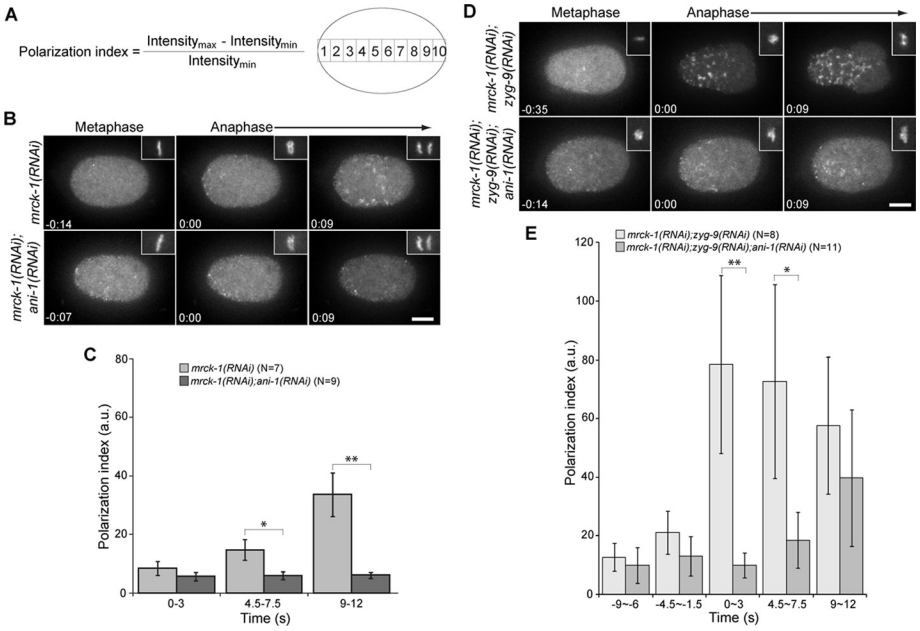

FIGURE 3: Anillin promotes the polarized accumulation of myosin. (A) Schematic and equation used to calculate a polarization index. (B) The distribution of cortical NMY-2::GFP in embryos depleted of MRCK-1 or both MRCK-1 and ANI-1 are shown during metaphase and anaphase. Cell cycle timing was determined by GFP::HIS (insets in the upper right of each frame). All images are projections of five planes spanning 2 µm. (C) Quantification of the GFP intensity in embryos acquired as in (B). (D) As in (B), but the embryos were additionally depleted of ZYG-9 to misposition the spindle in the posterior. (E) Quantification of the GFP intensity in embryos acquired as in (D). Error bars represent ± SEM. *, $p < 0.05$; **, $p < 0.01$ from paired *t* tests. Scale bars: 10 µm.

we compared the patterning of NMY-2::GFP foci in *zyg-9(b244ts)* and *zyg-9(b244ts); ani-1(RNAi)* embryos. NMY-2::GFP foci in the vicinity of the posterior spindle in *zyg-9(b244ts)* embryos were dim and failed to coalesce, comparable to the NMY-2::GFP foci in the entire cortex of *zyg-9(b244ts); ani-1(RNAi)* embryos (Figure 2, A and C, and Supplemental Fig2Video1). The similar behavior of NMY-2::GFP foci in anillin-depleted embryos and in the microtubule-dense regions of control and ZYG-9–depleted embryos suggests astral microtubules could inhibit the coalescence of cortical myosin by negatively regulating anillin.

Anillin recruitment is largely myosin-independent

To determine how anillin controls myosin recruitment, and how it contributes to the spatial regulation of myosin recruitment, we examined the localization of anillin itself. In wild-type *C. elegans* embryos, the distribution of cortical anillin resembles that of cortical myosin and there is extensive colocalization (Maddox *et al.*, 2005). Like myosin, anillin was recruited to the cortex in a polarized manner upon anaphase onset and then coalesced to form large foci in the equatorial region and at the anterior pole (Figures 2D, S1, S2, B and C, and Supplemental Fig4Video1). Depletion of the centrosomal component SPD-5 to prevent assembly of a normal mitotic spindle resulted in accumulation of ANI-1::GFP foci over the entire cortex, as observed with myosin (Figure 2, A and D). Given the colocalization of anillin and myosin during cytokinesis, and the anillin-dependent organization of cortical myosin (Maddox *et al.*, 2005), we examined whether depletion of myosin impacts anillin localization. In embryos depleted of NMY-2 to an extent sufficient to prevent cleavage furrow formation, GFP::ANI-1 was recruited to the equatorial region upon anaphase onset (Figure 2D). The anterior enrichment was not pronounced, but this was expected, because NMY-2 depletion disrupts the asymmetric positioning of the spindle (Guo and Kemphues, 1996). To assess whether GFP::ANI-1 accumulation is modulated by microtubule density in NMY-2–depleted embryos, we codepleted NMY-2 and ZYG-9 to induce a posterior spindle. Under these conditions, large foci of GFP::ANI-1 accumulated in a highly polarized manner, similar to control embryos depleted of ZYG-9 alone (Figures 2D and S1). These data suggest microtubules influence anillin localization independent of myosin and cortical contractility.

Anillin regulates myosin polarization during anaphase

To quantitatively assess whether anillin regulates the distribution of cortical myosin upon anaphase onset, we measured cortical myosin levels along the AP axis in control embryos expressing NMY-2::GFP and GFP::HIS. We measured the average NMY-2::GFP intensity in each of 10 equal-sized regions along the AP axis and calculated a polarization index reflecting the differential myosin recruitment among these regions (Figure 3A). Although myosin foci accumulated upon anaphase onset in a polarized manner in control embryos (Supplemental Fig2Video1), the myosin polarization index remained constant up to 12 s after anaphase onset (Figure S2A). This lack of change was due to the persistence of an anterior myosin cap from the maintenance phase of polarization that dissipated during anaphase coincident with the appearance of postanaphase foci (Werner *et al.*, 2007). To eliminate this anterior cap, we depleted MRCK-1, a CDC-42–dependent kinase (Kumfer *et al.*, 2010; Figure 3B). The anaphase-specific accumulation of NMY-2::GFP foci was unaffected by MRCK-1 depletion and myosin was primarily recruited to the equatorial and anterior regions as in control embryos (Figure 3B and Supplemental Fig3Video1; compare to Figures 2A and S2 and Supplemental Fig2Video1). Likewise, NMY-2::GFP foci accumulated and coalesced in the anterior cortex of *mrck-1(RNAi);zyg-9(RNAi)* embryos (Figure 3D and Supplemental Fig3Video1). Coalescence of NMY-2::GFP foci depended upon ANI-1 in MRCK-1–depleted embryos (Figure 3, B and D, and Supplemental Fig3Video1). In addition, anillin recruitment was largely unaffected by MRCK-1 depletion (Figure S2, B and C, and Supplemental Fig2Video1). Thus, MRCK-1 depletion only affected cortical myosin recruitment prior to anaphase.

We measured myosin accumulation along the AP axis in *mrck-1(RNAi)*, *mrck-1(RNAi);ani-1(RNAi)*, *mrck-1(RNAi);zyg-9(RNAi)*, and *mrck-1(RNAi);zyg-9(RNAi);ani-1(RNAi)* embryos (Figure S3) and calculated polarization indices. Within 3 s of anaphase onset, myosin was recruited to the cortex in both *mrck-1(RNAi)* embryos and *mrck-1(RNAi);ani-1(RNAi)* embryos (Figure 3C), however, the recruitment was polarized in *mrck-1(RNAi)* embryos, but not in *mrck-1(RNAi); ani-1(RNAi)* embryos (Figure 3C). In addition, myosin accumulation was highly polarized in *mrck-1(RNAi);zyg-9(RNAi)* embryos, but the recruitment was less polarized in *mrck-1(RNAi);zyg-9(RNAi);ani-1(RNAi)* embryos (Figure 3E). This analysis revealed that anillin contributes to the spatial regulation of cortical

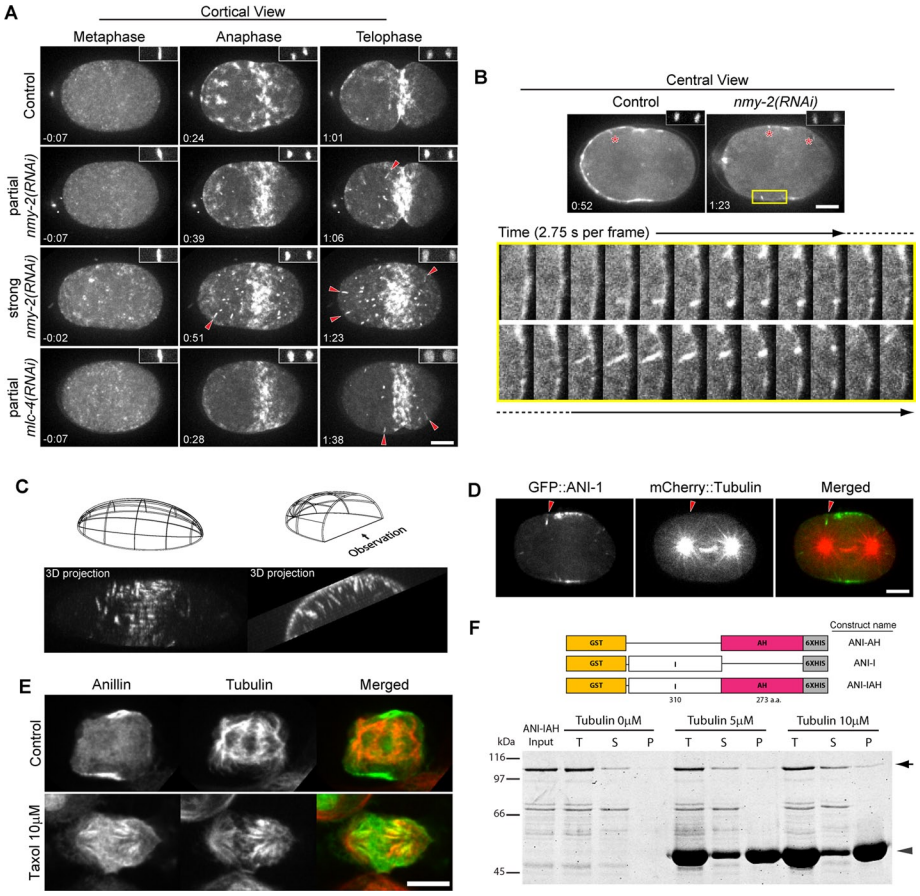

FIGURE 4: Anillin associates with microtubules. (A) Selected images from time-lapse sequences of embryos expressing GFP::ANI-1 (projections of 11 planes spanning 5 μm) at the indicated cell cycle phases. Time relative to anaphase onset is shown, and the insets show the chromatin imaged with mCherry:HIS. In embryos partially (cytokinesis-competent) or severely depleted of NMY-2 or the myosin regulatory light chain, MLC-4, radially distributed linear structures are observed near the cortex (red arrowheads). (B) Embryos like those in (A) were imaged at central planes (projection of three planes spanning 1 μm). Linear structures are also observed with this imaging modality (shown with red asterisks). High-magnification views of the yellow box region demonstrating the origin of linear structures at high time resolution. Dashed line indicates frames repeated at top and bottom rows. (C) Z-stacks were collected halfway through an embryo strongly depleted of NMY-2 and expressing GFP::ANI-1. Maximum intensity projections at the indicated times are shown as three-dimensional reconstructions of the data set from two different perspectives: from the side and end-on view from the anterior, as indicated in the schematics. (D) Embryo partially depleted of NMY-2 and expressing GFP::ANI-1 (green) and mCherry::tubulin (red) were imaged at a central plane (projection of three planes spanning 1 μm). The linear GFP::ANI-1 structures were collinear with the microtubules. Arrowheads indicate the linear structures. (E) Immunofluorescence of control or Taxol-treated (10 μM) HeLa cells during anaphase revealing the distribution of anillin (green) and microtubules (red). (F) Schematic of three ANI-1 expression constructs and a Coomassie Blue–stained SDS–PAGE of the microtubule cosedimentation assays. T: total fraction; S: supernatant fraction after ultracentrifugation; P: pellet fraction after ultracentrifugation; arrow on right: full-length ANI-IAH; arrowhead: Taxol-stabilized microtubules. Scale bars: 10 μm.

myosin recruitment, in addition to controlling the organization of cortical myosin foci.

To gain insight into how anillin can promote myosin accumulation, we compared the stability of myosin patches in the presence of and following depletion of anillin during anaphase. Myosin foci were identified using automated particle tracking (Sbalzarini and Koumoutsakos 2005). A fixed threshold was set to categorize foci into two intensity classes (dim or bright). In both control and ANI-1–depleted embryos, the majority of foci were dim and persisted for an average of 8 s (Figure S4). Control embryos contained more bright foci than anillin-depleted embryos, and these persisted for an average of three times longer than the small foci (Figure S4). We used fluorescence recovery after photobleaching to examine exchange of myosin in the foci, but we did not detect appreciable recovery of fluorescence to these foci during their short lifetime in ANI-1–depleted or control embryos (unpublished data). These results indicate that anillin promoted cortical myosin accumulation by promoting myosin coalescence into large foci that did not exhibit significant exchange of myosin.

Collectively, the data shown indicate that the accumulation of both myosin and anillin inversely correlates with the position of the microtubule asters. In addition, the inverse correlation between cortical anillin recruitment and microtubules was largely unaffected by myosin depletion, whereas depletion of anillin significantly impaired the polarization of myosin. On the basis of these data, we propose that microtubules inhibit the ability of anillin to promote myosin organization and stabilization. There are many possible underlying molecular mechanisms, but the simplest inhibitory mechanism is sequestration of anillin by microtubule binding. To investigate this possibility, we examined GFP::ANI-1 in control embryos and in posteriorly localized spindles of embryos. We could occasionally, but not reproducibly, observe linear elements of anillin in the vicinity of the spindle (unpublished data). To a first approximation, our inability to detect a clear association of anillin with microtubules as anillin and myosin become polarized argues against a sequestration model for inhibition of anillin function. However, this model should not be completely excluded, because anillin associates with microtubules in a number of contexts (see next section).

Anillin associates with microtubules

In the course of examining the distribution of GFP::ANI-1 in myosin-depleted embryos, we observed filamentous structures that extended perpendicular from the cortex (Figure 4, A–C, and Supplemental Fig4Video1). These structures appeared primarily during late anaphase/early telophase, after the initial cortical polarization, and were most frequently, though not exclusively, observed in the anterior half of the embryo. These observations indicate GFP::ANI-1 can localize in the cytoplasm, at the cortex, and in a previously undetected subcortical site.

The linear structures pointed toward the centrosome, and they were highly dynamic, suggesting they may represent anillin bound to microtubules. Imaging with high time resolution demonstrates that these structures appear at sites with preexisting cortical GFP::ANI-1 foci that elongate, intensify, and subsequently shrink

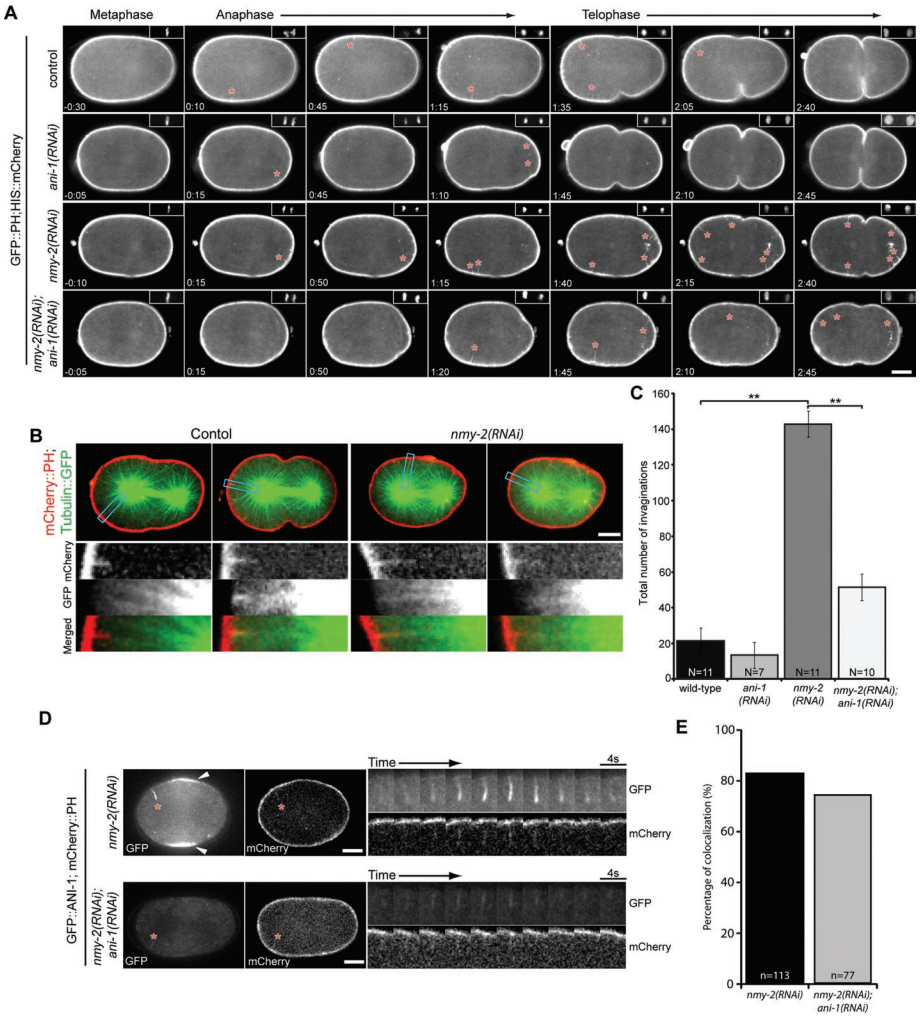

FIGURE 5: Anillin mediates microtubule–plasma membrane cortical interactions. (A) Selected images from time-lapse sequences of the center plane of embryos expressing GFP::PH (projection of three planes spanning 1 µm) at the indicated time relative to anaphase onset is shown (insets show the chromatin as detected with mCherry::HIS). Small, local, transient cortical invaginations (indicated by red asterisks) are observed in control embryos and some ANI-1–depleted embryos. (B) Dual-color confocal imaging of mCherry::PH and GFP::tubulin. Boxed regions are shown below the embryos at high magnification. (C) Total number of cortical invaginations from t = 0–180 s as from embryos in (A). (D) Selected images from time-lapse sequences of embryos expressing GFP::ANI-1 and mCherry::PH following depletion of NMY-2 alone or both NMY-2 and ANI-1. Cortical invaginations are indicated by red asterisks. GFP::ANI-1 accumulated to the equatorial cortex in NMY-2–depleted embryos (white arrowheads) but not in embryos depleted of both NMY-2 and ANI-1. Time-lapse sequences of the indicated (*) invaginations are shown at high magnification. (E) Invaginations detected by mCherry::PH were scored for the presence of GFP::ANI-1 in embryos as shown in (D). Error bars are ± SEM. **, $p < 0.05$ by paired *t* test. Scale bars: 10 µm.

to the cortex and disappear (Figure 4B and Supplemental Fig4Video1&2). Because strong depletion of a major cytokinetic component may result in nonspecific effects, we examined whether the filamentous structures could form in embryos partially depleted of myosin and capable of forming cleavage furrows. GFP::ANI-1 filamentous structures are also frequently observed in cleavage-competent *nmy-2(RNAi-partial)* embryos (Figure 4A and Supplemental Fig4Video1&2). These structures were also observed when cortical myosin levels were perturbed in embryos depleted of the regulatory light chain of myosin, MLC-4 (Figure 4A and Supplemental Fig4Video1). More infrequently, these structures could also be observed in control embryos expressing GFP::ANI-1 (Figure 4B). These results indicate a novel localization pattern of GFP::ANI-1.

To determine whether these linear forms of anillin are microtubule-associated, we examined ANI-1 localization in embryos coexpressing GFP::ANI-1 and mCherry::tubulin. In *nmy-2(RNAi-partial)* embryos, GFP::ANI-1 decorated the ends of some microtubules (Figure 4D). Furthermore, we labeled GFP::ANI-1 and endogenous tubulin in fixed *nmy-2(RNAi)* embryos and found GFP::ANI-1 localized at microtubule plus ends (Figure S5). We conclude that anillin can associate with microtubules during anaphase.

To examine whether the ability to associate with microtubules is a conserved property of anillin, we examined the localization of anillin in dividing HeLa cells. In unperturbed cells, anillin is highly concentrated at the cleavage furrow, as previously described (Oegema *et al.*, 2000; Figure 4E). As Taxol treatment has been previously shown to induce redistribution of several cytokinesis proteins (Hummer and Mayer, 2009), we examined anillin localization in Taxol-treated anaphase cells and found that anillin redistributed from the cell cortex to spindle microtubules (Figure 4E). Thus, microtubule association, either direct or indirect, appears to be a conserved property of anillin.

To determine whether anillin binds directly to microtubules, we constructed three different N-terminal GST- and C-terminal HIS-tagged anillin fragments, expressed them, and examined whether they cosedimented with microtubules (Figure 4F). Truncated anillin (ANI-IAH), lacking the N-terminal myosin- and actin-binding domains and the C-terminal PH domain, sedimented with Taxol-stabilized microtubules in a tubulin concentration–dependent manner (Figure 4F). Neither the proteolytic fragments of ANI-IAH (Figure 4F), nor the other anillin constructs, nor GST alone cosedimented with microtubules (unpublished data). This fragment did not quantitatively sediment, suggesting a relatively weak affinity for microtubules.

Anillin mediates microtubule–cell cortex association during anaphase

A recent report (Redemann *et al.*, 2010) demonstrated plasma membrane invaginations in *C. elegans* embryos expressing the plasma membrane markers GFP::PH or mCherry::PH. Interestingly, the authors reported that the abundance of these invaginations increased dramatically upon depletion of NMY-2, as we have observed for the association of GFP::ANI-1 with microtubules. Using these membrane markers, we reproduced the fine linear structures extending toward the centrosome in control cells (Figure 5A and Supplemental Fig5Video1). Coexpression of mCherry::PH and GFP::tubulin revealed that the invaginations detected with

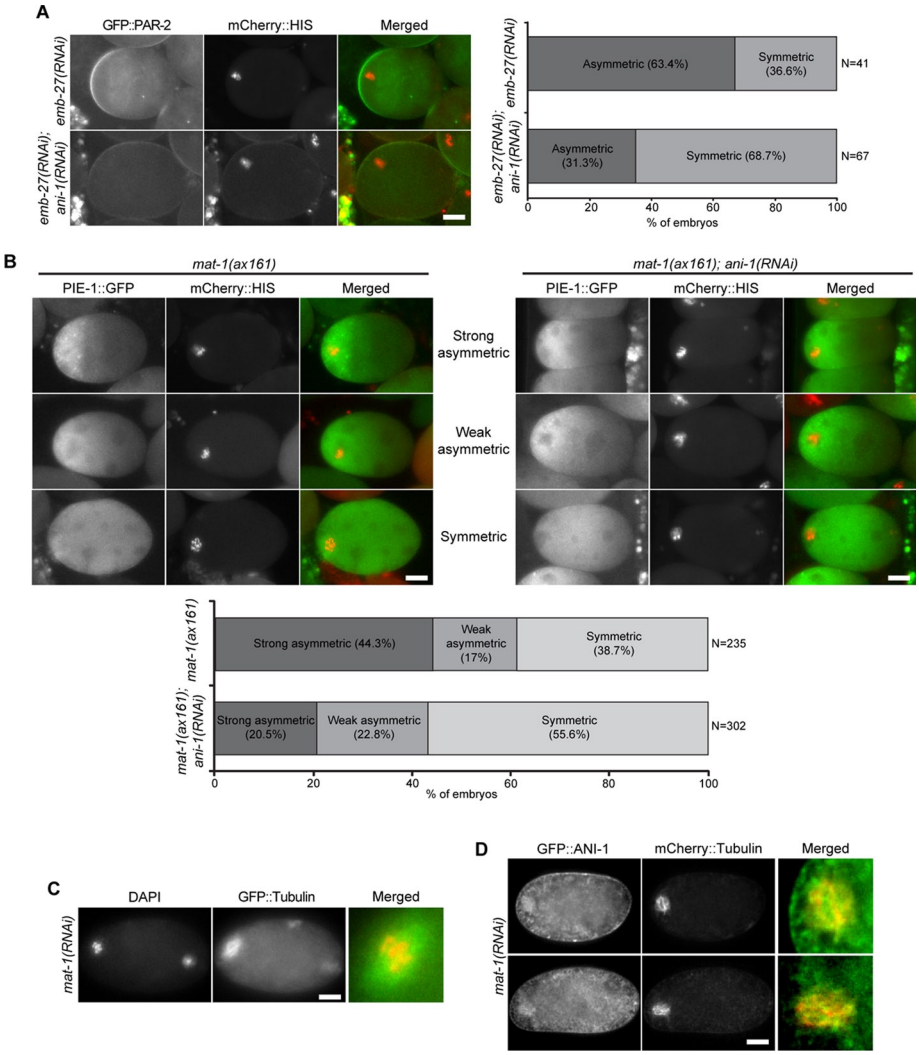

FIGURE 6: Anillin concentrates on meiotic spindles and contributes to cell polarization. (A) GFP::PAR-2 distribution in control and ANI-1–depleted oocytes arrested in meiosis I due to EMB-27 depletion. (B) PIE-1::GFP distribution in control and ANI-1–depleted *mat-1(ax161)* oocytes arrested at the restrictive temperature in meiosis I. (C) Overview of the microtubule cytoskeleton in meiotically arrested oocytes. MAT-1–depleted, GFP::tubulin-expressing oocytes were stained with DAPI in M9 buffer. (D) GFP::ANI-1 distribution in fertilized oocytes defective for the APC/C due to depletion of *mat-1(ax161)* conditional mutation. Scale bars: 10 μm.

mCherry::PH were colinear with microtubules that approach the cell cortex (Figure 5B). The structures observed with GFP::PH might reflect a general property of cortex–microtubule interactions. Alternatively, anillin may play a crucial role in their formation. To examine whether the GFP::PH invaginations are related to those observed with GFP::ANI-1, we simultaneously imaged GFP::ANI-1 and mCherry::PH in NMY-2–depleted embryos, in which the structures are abundant. Both markers could be detected in the vast majority of invaginations, but they did not precisely overlap. The GFP::ANI-1 signal extended more internally than the mCherry::PH signal. The consistent cooccurrence of the two markers in the invagination is remarkable, because mCherry::PH labeled the plasma membrane quite continuously, but GFP::ANI-1 was localized in a highly punctate manner, suggesting that anillin could be required for formation of the invaginations. We therefore measured the abundance of these structures in ANI-1–depleted embryos. As these invaginations are relatively infrequent in *ani-1(RNAi)* and control embryos, we quantitated the anillin dependence of these invaginations in cells depleted of NMY-2, which results in a sevenfold increase in their abundance (Figures 5, A and C, and S6 and Supplemental Fig5Video1; Redemann *et al.*, 2010). The invaginations were threefold less abundant in embryos codepleted of ANI-1 and NMY-2, as compared with embryos depleted of NMY-2 alone (Figures 5, A and C, and S6 and Supplemental Fig5Video1). We examined whether residual anillin might be associated with the remaining invaginations despite being significantly depleted (70%). Indeed, when both ANI-1 and NMY-2 were depleted from embryos expressing both GFP::ANI-1 and mCherry::PH, residual GFP::ANI-1 was clearly detectable in ~75% of the remaining invaginations (Figure 5, D and E). As ANI-1 promoted formation of the invaginations, and the protein was present in the majority of all invaginations, we conclude that ANI-1 can link cortical factors to microtubules.

Anillin can contribute to cell polarization in meiosis

To examine whether anillin has a role in cell polarization in another context in which microtubules serve as a polarizing cue, we turned to fertilized oocytes arrested in meiosis I. Fertilized oocytes arrested in meiosis I due to inactivation of the anaphase-promoting complex (APC) exhibit polarity inversion induced by the meiotic spindle in a microtubule-dependent manner (Wallenfang and Seydoux, 2000; Figure S7A). Polarity inversion can be monitored by scoring the accumulation of posterior PAR proteins, such as PAR-2, on the cortex adjacent to the meiotic spindle and by scoring asymmetric accumulation of GFP::PIE-1, a maternally deposited transcriptional repressor that segregates with the germ lineage in early embryos (Mello *et al.*, 1996; Seydoux *et al.*, 1996). We used depletion or mutation of APC subunits MAT-1 or EMB-27 in conjunction with depletion of ANI-1 to investigate whether anillin is involved in this model for cell polarization. GFP::PAR-2 was asymmetrically localized in ~60% (n = 69) of fertilized oocytes depleted of EMB-27 alone, but in only ~30% (n = 65) of fertilized oocytes depleted of both ANI-1 and EMB-27 (Figure 6A). We next assessed whether ANI-1 contributes to the asymmetric distribution of PIE-1. Whereas GFP::PIE-1 was asymmetrically distributed in 61% of *mat-1(ax161)* oocytes, GFP::PIE-1 was asymmetric in 43% of *mat-1(ax161);ani-1(RNAi)* oocytes (Figure 6B). Thus anillin promoted the polarization of fertilized oocytes in response to the meiotic spindle.

These fertilized oocytes contained a meiotic spindle composed of a dense array of microtubules surrounding the maternal chromatin and few other microtubules (Figure 6C). To examine whether anillin localizes to the meiotic spindle, we imaged GFP::ANI-1 in live *mat-1(ax161)* oocytes immediately upon dissection. We observed GFP::ANI-1 was distinctly concentrated on the spindle (Figure 6D). Examination of anillin truncations revealed that both N- and C-terminally truncated anillin could also associate with the microtubules

of the meiotic spindle (Figure S7B), suggesting that the primary determinant of microtubule association lies in its central region. Thus, during the microtubule-directed polarization of meiotically arrested, fertilized oocytes, ANI-1 concentrates on the meiotic spindle and contributes to oocyte polarization.

DISCUSSION

On anaphase onset, the equatorial accumulation of cortical myosin II and the subsequent formation of a cleavage furrow is dictated by the combined action of a positive cue from the central spindle and an inhibitory cue from astral microtubules. A molecular framework for the nature of the positive cue has been described (Piekny *et al.*, 2005), but the molecules involved in the inhibitory cue remain obscure. In this paper, we have demonstrated that the inhibition of cortical myosin recruitment by astral microtubules in the early *C. elegans* embryo involves the cytoskeletal scaffold protein anillin, which has the capacity to bind to microtubules.

Anillin contributes to cell polarization

During anaphase, cortical myosin accumulates in a highly polarized manner. In particular, cortical myosin inversely correlates with the proximity of microtubules to the cell cortex. Repositioning of the spindle redirects the polarized accumulation of myosin, strengthening this inverse correlation (Werner *et al.*, 2007). In regions where microtubules are less dense—or in the entire embryo if centrosome assembly is prevented—myosin coalesces into larger foci that persist for longer than small myosin foci. This coalescence of myosin into larger foci requires anillin, as does the polarized accumulation of myosin. Like myosin, the cortical recruitment of anillin is polarized. Whereas myosin polarization requires anillin, anillin can accumulate in a polarized manner in cells depleted of myosin. We propose that the polarized accumulation of anillin promotes the polarized recruitment of myosin.

Not only does anillin promote the formation of the aster-directed furrow, it also contributes to the ability of the meiotic spindle to direct asymmetric accumulation of PAR-2 and PIE-1 in arrested oocytes. However, anillin is unlikely to be the sole mediator of either astral inhibition or oocyte polarization. Anterior-directed myosin flows are detectable in ANI-1–depleted embryos, indicating residual asymmetry. Likewise, anillin depletion does not abrogate PAR-2 recruitment to the cortex adjacent to the meiotic spindle.

The polarized accumulation of myosin that facilitates cytokinesis during anaphase shares several properties with the polarized accumulation of myosin that facilitates embryo polarization upon fertilization. The dynamics of cortical myosin are similar during these two processes, and there is a common requirement for several proteins. In addition to ANI-1, these include the protein phosphatase PPH-6 and its associated subunit SAPS-1, as well as wild-type levels of the formin CYK-1 and the RhoGEF ECT2 (Werner *et al.*, 2007; Werner and Glotzer, 2008; Afshar *et al.*, 2010; Zonies *et al.*, 2010). One apparent difference between these processes is the initial cue that leads to either the anterior accumulation of myosin during polarization or the equatorial accumulation of myosin during cytokinesis. In the latter case, microtubule asters provide the positional information, whereas in the former case, the process is initiated by the sperm centrosome in a microtubule-independent manner (Cowan and Hyman, 2004; Sonneville and Gonczy, 2004), although there is some evidence that the centrosome cue can involve microtubules (Tsai and Ahringer, 2007). Irrespective of the mechanism of symmetry breaking, microtubule-mediated inhibition of anillin could further enhance differential myosin recruitment and promote the formation of a deeply ingressing furrow.

Anillin associates with microtubules

Our results indicate that microtubules inhibit cortical recruitment of anillin in microtubule-rich regions of the embryo. From our global depletion studies, we infer that regional inhibition of anillin would result in regional inhibition of myosin accumulation. What molecular mechanism could mediate the regional inhibition of cortical anillin recruitment? There are a number of possible mechanisms, including, but not limited to, local sequestration by binding to microtubules, microtubule-directed posttranslational modification, or local inhibition of a critical cofactor. Although our results do not discriminate among these possible mechanisms, we note that local sequestration of anillin is the simplest model, and we have also demonstrated that anillin has a conserved capacity to associate with microtubules, which is a prerequisite for the sequestration model.

When we examined anillin localization in nonmuscle myosin-depleted embryos, we observed intense anillin labeling of a subset of microtubules during late anaphase. These labeled microtubules were also associated with invaginations of the plasma membrane. These invaginations were far less abundant when anillin was depleted and the remaining invaginations were highly enriched in residual anillin, suggesting that anillin is required to link microtubules to the membrane, rather than being a passive component. Anillin also concentrates on the meiotic spindle in arrested oocytes. An interaction between anillin and microtubules is also detectable in human cells. Direct binding of anillin to microtubules can be reconstituted with purified components; however, additional factors may participate in vivo. Collectively, these diverse observations indicate that anillin associates with microtubules, either directly or indirectly.

Indeed, anillin has been previously shown to associate with microtubules in vitro. *Drosophila* anillin was found in an early proteomics screen for proteins that bind to both F-actin and Taxol-stabilized microtubules (Sisson *et al.*, 2000). More recently, in *Drosophila* cells treated with actin-depolymerizing agents, anillin was observed to form extended filamentous structures, some of which could associate with the extreme plus ends of microtubules (D'Avino *et al.*, 2008; Hickson and O'Farrell, 2008). The binding of anillin to stabilized microtubules may well explain the recent finding that Taxol treatment during anaphase (Rankin and Wordeman, 2010) induces the remarkable cortical oscillations that are a distinguishing feature of anillin-depleted cells (Straight *et al.*, 2005; Zhao and Fang, 2005; Piekny and Glotzer, 2008). Thus, although anillin is a prominent cortical component, it can also associate with microtubules in *C. elegans*, *Drosophila*, and mammalian cells, under certain conditions.

Given the conserved capacity of anillin to associate with microtubules, and the observation that anillin recruitment anticorrelates with microtubule density, we speculate that microtubules could sequester anillin and prevent its recruitment to the cortex, where it organizes and stabilizes myosin. In this model, microtubule and cortex recruitment are predicted to be mutually exclusive, which is consistent with the finding that depletion of myosin enhances the association of anillin with microtubules. However, it has proven difficult to detect the association of anillin with microtubules during early anaphase, as myosin becomes polarized. The association of soluble anillin with the large number of astral microtubules may result in only a weak enrichment over background, as opposed to the bright labeling that results from the large multisubunit particles that associate with microtubule tips at the cell cortex. However, anillin can be easily and reproducibly detected on the dense microtubules of the meiotic spindle, indicating that cortical enrichment is not a prerequisite for microtubule association.

Further evidence for anillin sequestration could come from measurements of the rate of anillin diffusion in microtubule-rich

and -depleted regions of the embryo. Proof that this mechanism is responsible for astral relaxation will require the generation of an anillin variant that is specifically defective in microtubule association.

MATERIALS AND METHODS

Strains

C. elegans strains (listed in Supplemental Table S1) were maintained using standard procedures on nematode growth medium (NGM) plates. Some nematode strains were provided by the Caenorhabditis Genetics Center, which is funded by the National Institutes of Health (NIH) National Center for Research Resources (NCRR).

RNA interference

All the RNA interference (RNAi) constructs were obtained from the RNAi feeding library of Ahringer and colleagues (Kamath *et al.*, 2003). All RNAi experiments were performed using the feeding method as described in Timmons and Fire (1998). Bacteria cultures were grown in Luria broth, and 200 µl was seeded on NGM plates containing 100 µg/ml ampicillin and 1 mM isopropyl β-D-1-thiogalactopyranoside (IPTG) and kept at room temperature for 8 h. For double and triple RNAi feeding experiments, bacteria cultures were mixed equally according to cell density, as measured by absorbance at 600 nm. Young L4 hermaphrodites were picked onto the plates for feeding at 25°C at least 24 h prior to examination.

Confocal microscopy

To prepare slides for imaging of *C. elegans* embryos, gravid hermaphrodites were dissected in egg salt buffer on coverslips, mounted on 2.5% agarose pads, and sealed with Vaseline. Embryos were imaged with a 63×/1.4 numerical aperture oil-immersion lens on a Zeiss Axiovert 200M equipped with a Yokogawa (Tokyo, Japan) CSU-10 spinning-disk unit (McBain) and illuminated with 50-mW, 473-nm and 25-mW, 561-nm lasers (Cobolt, Solna, Sweden). Images were captured on a Cascade 512B EM-CCD camera (Photometrics, Tucson, AZ) controlled by MetaMorph (Molecular Devices, Sunnyvale, CA). Image processing was performed with ImageJ (http://rsb.info.nih.gov/ij/).

For the live imaging of embryos expressing GFP::PH in Figure 1, we acquired GFP and Nomarski images at the embryo center every 5 s, with 250-ms exposure time. For Figures 2 and 3, we imaged live embryos expressing NMY-2::GFP and GFP::HIS continuously with five cortical planes spanning 2 µm and a single central plane. GFP exposure times were 250 ms. For the montage analysis in Figure 2C, we selected a region in 220 × 30 pixels along the AP axis of the embryos from every fifth time point, and generated montages using MetaMorph and ImageJ. In Figure 4A, we imaged live embryos continuously with 11 cortical planes spanning 5 µm and a single central plane. Exposure times were 200 ms for GFP and 250 ms for mCherry. In Figure 4B, we imaged live embryos continuously around the center with three frames (0.5-µm increments, 1 µm in total) for GFP and a single plane for mCherry. Exposure times were 500 ms for GFP 250 ms for mCherry. For imaging the embryos expressing GFP::PH and mCherry::HIS in Figure 5, we acquired three planes spanning 1 µm in the center for GFP and a single central plane for mCherry; images were acquired at 5 s intervals. In Figure 5D, we continuously acquired a 1-s GFP image followed by a 1.5-s mCherry image at a central focal plane.

To prepare slides for imaging of meiotically arrested *C. elegans* oocytes in Figure 6, hermaphrodites were dissected in M9 buffer on coverslips, mounted on 2.5% agarose pads, and sealed with Vaseline. We acquired five central planes spanning 5 µm for both GFP (2-s exposure) and mCherry (500-ms exposure); a single plane was selected and presented.

All Z-stacks were projected with a maximum-intensity algorithm. Resulting time-lapse projections were assembled into movies using MetaMorph and ImageJ. To visualize three-dimensional image stacks from arbitrary positions, Z-stacks were converted to 8-bit TIFFs with ImageJ, and further processed with Osirix (Pixmeo, Geneva, Switzerland).

Epifluorescence microscopy

To prepare slides for imaging of meiotically arrested *C. elegans* oocytes in Figure 6, A and E, we dissected gravid hermaphrodites in M9 buffer on coverslips mounted on glass slides, with Vaseline on the corners to prevent overcompression and as a sealant. Fertilized oocytes were imaged with a 40×/0.75 numerical aperture oil-immersion lens on a Zeiss AxioImager (Jena, Germany) M1 microscope. Images were captured on a Cascade 1K EM-CCD camera (Photometrics) controlled by MetaMorph. Image processing was performed with ImageJ. We acquired all images with a single plane around the center of the oocytes. Exposure times for GFP and mCherry were 500 ms. For MAT-1–depleted embryos expressing GFP::tubulin in Figure 6, C and D, we stained the embryos with DAPI in M9 buffer (1:1000) for 5 min to visualize chromatin before imaging.

Cell culture, drug treatment, and immunostaining

To perform drug treatment, we cultured HeLa cells on six-well culture plates to 80% confluence. *S*-trityl-L-cysteine (STC; 2.5 µM) was added, and the plates were incubated for 6 h, after which 10 µM Taxol was added. After 10 min, 22.5 µM purvalanol was added, and the plates were incubated for another 30 min. The cells were then fixed in methanol at −20°C for 30 min and washed with phosphate-buffered saline Tween-20 (PBST). The fixed cells were further subjected to blocking solution (phosphate-buffered saline [PBS] with 5% goat serum) for an hour. A mixture of anillin antisera (rabbit) at 1:200 and mouse anti-DM1α antibodies at 1:500 were used as primary antibodies, followed by detection with rabbit Alexa Fluor 488 and mouse Alexa Fluor 568. Cells were mounted in Fluoromount G (Southern Biotechnology, Birmingham, AL) and imaged by the epifluorescence microscopy system described in the preceding section.

Recombinant protein expression and purification

Truncated anillin constructs, ANI-AH, ANI-I, and ANI-IAH, were amplified and inserted into the pGEX-TEV vector and expressed in BL21 (DE3) RIl cells. Protein expression was induced by the addition of 0.4 mM IPTG at 25°C for 7–8 h. Bacteria were harvested and resuspended in 10 mM HEPES (pH 7.7), 50 mM NaCl, 1 mM ethylene glycol tetraacetic acid (EGTA), 1 mM MgCl2, 0.1% Triton-X 100, 1 mM dithiothreitol (DTT), 0.1 mM ATP, 10 mg/ml leupeptin/pepstatin, and 1 mM phenylmethylsufonylflouride containing 0.5 mg/ml lysozyme prior to sonication. Lysates were centrifuged in a JA.20 Beckman rotor at 18,000 rpm at 4°C for 20 min. Prewashed glutathione-agarose beads were added to the cleared lysates and incubated at 4°C for 2 h with mixing. Following washes, proteins were eluted with 20 mM glutathione in HEPES buffer. The purified recombinant proteins were stored in aliquots at −80°C.

Sedimentation assay and SDS–PAGE

To perform the tubulin sedimentation assay, 0.1 M GTP and 0.25 M $MgCl_2$ were added to recycled tubulin and centrifuged

at 80,000 rpm for 10 min at 4°C. The precleared, recycled tubulin was then polymerized in 2 mM GTP, 24% glycerol in 1X BRB-80 buffer, and 40 μM Taxol for 30 min. Purified recombinant proteins were added to the Taxol-stabilized microtubules and incubated for 45 min at room temperature with gentle mixing. 20 μl of total 100 μl reaction mixtures was sampled ("total"). The remaining reaction mixture was loaded onto the top of a 48% sucrose cushion and centrifuged at 40,000 rpm for 10 min, after which 30 μl of supernatant was collected ("supernatant"). The resulting pellet was washed twice with 1X BRB-80 buffer and resuspended in 80 μl 1X BRB-80 buffer ("pellet" fraction). Equal amounts of total, supernatant, and pellet fractions were loaded into 8% SDS–PAGE gel. The resulting gel was stained with Coomassie Blue.

Image quantification

For measurements of the extent of the membrane ingression in ZYG-9 mutant embryos expressing GFP::PH (Figure 1), we manually selected the images with maximum membrane ingression using ImageJ. For embryos with anterior furrows, we used ImageJ to measure the distance between the two furrow tips. For embryos without anterior furrows, we measured the distance between the anterior cortices at one-third egg length (Figure 1). The ingression percentage was calculated by the equation shown in Figure 1C.

To measure the myosin intensity upon anaphase onset in the embryos as shown in Figure 3, we divided the AP axis of the embryos into 10 equal regions in each projected image (five planes spanning 2 μm) and measured the average intensities in each region using MetaMorph. The data were exported to Excel (Microsoft, Redmond, WA) for further analysis. Polarization index was calculated using the equation shown in Figure 3A.

For measurement of the number of invaginations in embryos expressing GFP::PH (Figure 5), we first adjusted the contrast of the projected images (three planes spanning 1 μm) in ImageJ to reduce the background and enhance the GFP signals, and then made binary images. We then used ABSnake in ImageJ to outline the inner cortex and reduced the size of the outline to 97%. After that, we pasted the scaled outlines as a line into the binary images and executed a line scan. The intensity data were further analyzed in Excel, and the number of intensity peaks were counted. Each intensity peak represents a single invagination. Peaks with a pixel width less than two were designated as noise and excluded from the measurement.

To count the number of embryos with symmetric/asymmetric distribution of GFP::PAR-2 and PIE-1::GFP in meiotically arrested oocytes (Figure 6, A and B), we selected the oocytes with condensed chromatin and classified the GFP distribution manually.

ACKNOWLEDGMENTS

We thank Amy Maddox for providing strains expressing truncated GFP::ANI-1 variants and for numerous helpful discussions throughout this project. We also thank Ed Munro for helpful discussions and the Ahringer lab for the strain expressing mCherry::tubulin. This work was supported by an NIH grant (R01-GM085087) to MG and the American Heart Association Midwest Postdoctoral Fellowship (09POST2110164) to Y.C.T.

REFERENCES

Afshar K, Werner ME, Tse YC, Glotzer M, Gonczy P (2010). Regulation of cortical contractility and spindle positioning by the protein phosphatase 6 PPH-6 in one-cell stage *C. elegans* embryos. Development 137, 237–247.

Alsop GB, Zhang D (2003). Microtubules are the only structural constituent of the spindle apparatus required for induction of cell cleavage. J Cell Biol 162, 383–390.

Audhya A, Hyndman F, McLeod IX, Maddox AS, Yates JR III, Desai A, Oegema K (2005). A complex containing the Sm protein CAR-1 and the RNA helicase CGH-1 is required for embryonic cytokinesis in *Caenorhabditis elegans*. J Cell Biol 171, 267–279.

Bement WM, Miller AL, von Dassow G (2006). Rho GTPase activity zones and transient contractile arrays. Bioessays 28, 983–993.

Bringmann H, Hyman AA (2005). A cytokinesis furrow is positioned by two consecutive signals. Nature 436, 731–734.

Burkard ME *et al.* (2009). Plk1 self-organization and priming phosphorylation of HsCYK-4 at the spindle midzone regulate the onset of division in human cells. PLoS Biol 7, e1000111.

Burkard ME, Randall CL, Larochelle S, Zhang C, Shokat KM, Fisher RP, Jallepalli PV (2007). Chemical genetics reveals the requirement for Polo-like kinase 1 activity in positioning RhoA and triggering cytokinesis in human cells. Proc Natl Acad Sci USA 104, 4383–4388.

Chartier NT, Salazar Ospina DP, Benkemoun L, Mayer M, Grill SW, Maddox AS, Labbe JC (2011). PAR-4/LKB1 mobilizes nonmuscle myosin through anillin to regulate *C. elegans* embryonic polarization and cytokinesis. Curr Biol 21, 259269.

Cowan CR, Hyman AA (2004). Centrosomes direct cell polarity independently of microtubule assembly in *C. elegans* embryos. Nature 431, 92–96.

D'Avino PP, Takeda T, Capalbo L, Zhang W, Lilley KS, Laue ED, Glover DM (2008). Interaction between Anillin and RacGAP50C connects the actomyosin contractile ring with spindle microtubules at the cell division site. J Cell Sci 121, 1151–1158.

D'Avino PP, Savoian MS, Glover DM (2005). Cleavage furrow formation and ingression during animal cytokinesis: a microtubule legacy. J Cell Sci 118, 1549–1558.

Dechant R, Glotzer M (2003). Centrosome separation and central spindle assembly act in redundant pathways that regulate microtubule density and trigger cleavage furrow formation. Dev Cell 4, 333–344.

Field CM, Alberts BM (1995). Anillin, a contractile ring protein that cycles from the nucleus to the cell cortex. J Cell Biol 131, 165–178.

Glotzer M (2009). The 3Ms of central spindle assembly: microtubules, motors and MAPs. Nat Rev Mol Cell Biol 10, 9–20.

Guo S, Kemphues KJ (1996). A non-muscle myosin required for embryonic polarity in *Caenorhabditis elegans*. Nature 382, 455–458.

Hamill DR, Severson AF, Carter JC, Bowerman B (2002). Centrosome maturation and mitotic spindle assembly in *C. elegans* require SPD-5, a protein with multiple coiled-coil domains. Dev Cell 3, 673–684.

Hickson GR, O'Farrell PH (2008). Rho-dependent control of anillin behavior during cytokinesis. J Cell Biol 180, 285–294.

Hummer S, Mayer TU (2009). Cdk1 negatively regulates midzone localization of the mitotic kinesin Mklp2 and the chromosomal passenger complex. Curr Biol 19, 607–612.

Kamath RS *et al.* (2003). Systematic functional analysis of the *Caenorhabditis elegans* genome using RNAi. Nature 421, 231–237.

Kumfer KT, Cook SJ, Squirrell JM, Eliceiri KW, Peel N, O'Connell KF, White JG (2010). CGEF-1 and CHIN-1 regulate CDC-42 activity during asymmetric division in the *Caenorhabditis elegans* embryo. Mol Biol Cell 21, 266–277.

Lewellyn L, Dumont J, Desai A, Oegema K (2010). Analyzing the effects of delaying aster separation on furrow formation during cytokinesis in the *Caenorhabditis elegans* embryo. Mol Biol Cell 21, 50–62.

Maddox AS, Habermann B, Desai A, Oegema K (2005). Distinct roles for two *C. elegans* anillins in the gonad and early embryo. Development 132, 2837–2848.

Maddox AS, Lewellyn L, Desai A, Oegema K (2007). Anillin and the septins promote asymmetric ingression of the cytokinetic furrow. Dev Cell 12, 827–835.

Matthews LR, Carter P, Thierry-Mieg D, Kemphues K (1998). ZYG-9, a *Caenorhabditis elegans* protein required for microtubule organization and function, is a component of meiotic and mitotic spindle poles. J Cell Biol 141, 1159–1168.

Mello CC, Schubert C, Draper B, Zhang W, Lobel R, Priess JR (1996). The PIE-1 protein and germline specification in *C. elegans* embryos. Nature 382, 710–712.

Munro E, Nance J, Priess JR (2004). Cortical flows powered by asymmetrical contraction transport PAR proteins to establish and maintain anterior-posterior polarity in the early *C. elegans* embryo. Dev Cell 7, 413–424.

Murthy K, Wadsworth P (2008). Dual role for microtubules in regulating cortical contractility during cytokinesis. J Cell Sci 121, 2350–2359.

Oegema K, Savoian MS, Mitchison TJ, Field CM (2000). Functional analysis of a human homologue of the *Drosophila* actin binding protein anillin suggests a role in cytokinesis. J Cell Biol 150, 539–552.
Petronczki M, Glotzer M, Kraut N, Peters JM (2007). Polo-like kinase 1 triggers the initiation of cytokinesis in human cells by promoting recruitment of the RhoGEF Ect2 to the central spindle. Dev Cell 12, 713–725.
Piekny A, Werner M, Glotzer M (2005). Cytokinesis: welcome to the Rho zone. Trends Cell Biol 15, 651–658.
Piekny AJ, Glotzer M (2008). Anillin is a scaffold protein that links RhoA, actin, and myosin during cytokinesis. Curr Biol 18, 30–36.
Piekny AJ, Maddox AS (2010). The myriad roles of Anillin during cytokinesis. Semin Cell Dev Biol 21, 881–891.
Rankin KE, Wordeman L (2010). Long astral microtubules uncouple mitotic spindles from the cytokinetic furrow. J Cell Biol 190, 35–43.
Redemann S, Pecreaux J, Goehring NW, Khairy K, Stelzer EH, Hyman AA, Howard J (2010). Membrane invaginations reveal cortical sites that pull on mitotic spindles in one-cell *C. elegans* embryos. PLoS One 5, e12301.
Sbalzarini IF, Koumoutsakos P (2005). Feature point tracking and trajectory analysis for video imaging in cell biology. J Struct Biol 151, 182–195.
Schenk C, Bringmann H, Hyman AA, Cowan CR (2010). Cortical domain correction repositions the polarity boundary to match the cytokinesis furrow in *C. elegans* embryos. Development 137, 1743–1753.
Seydoux G, Mello CC, Pettitt J, Wood WB, Priess JR, Fire A (1996). Repression of gene expression in the embryonic germ lineage of *C. elegans*. Nature 382, 713–716.
Sisson JC, Field C, Ventura R, Royou A, Sullivan W (2000). Lava lamp, a novel peripheral Golgi protein, is required for *Drosophila melanogaster* cellularization. J Cell Biol 151, 905–918.
Sonneville R, Gonczy P (2004). *zyg-11* and *cul-2* regulate progression through meiosis II and polarity establishment in *C. elegans*. Development 131, 3527–3543.
Srayko M, Kaya A, Stamford J, Hyman AA (2005). Identification and characterization of factors required for microtubule growth and nucleation in the early *C. elegans* embryo. Dev Cell 9, 1506–1511.
St Johnston D, Ahringer J (2010). Cell polarity in eggs and epithelia: parallels and diversity. Cell 141, 757–774.
Straight AF, Field CM, Mitchison TJ (2005). Anillin binds nonmuscle myosin II and regulates the contractile ring. Mol Biol Cell 16, 193–201.
Timmons L, Fire A (1998). Specific interference by ingested dsRNA. Nature 395, 854.
Tsai MC, Ahringer J (2007). Microtubules are involved in anterior-posterior axis formation in *C. elegans* embryos. J Cell Biol 179, 397–402.
von Dassow G, Verbrugghe KJ, Miller AL, Sider JR, Bement WM (2009). Action at a distance during cytokinesis. J Cell Biol 187, 831–845.
Wallenfang MR, Seydoux G (2000). Polarization of the anterior-posterior axis of *C. elegans* is a microtubule-directed process. Nature 408, 89–92.
Watanabe S, Okawa K, Miki T, Sakamoto S, Morinaga T, Segawa K, Arakawa T, Kinoshita M, Ishizaki T, Narumiya S (2010). Rho and anillin-dependent control of mDia2 localization and function in cytokinesis. Mol Biol Cell 21, 3193–3204.
Werner M, Glotzer M (2008). Control of cortical contractility during cytokinesis. Biochem Soc Trans 36, 371–377.
Werner M, Munro E, Glotzer M (2007). Astral signals spatially bias cortical myosin recruitment to break symmetry and promote cytokinesis. Curr Biol 17, 1286–1297.
Wolfe BA, Takaki T, Petronczki M, Glotzer M (2009). Polo-like kinase 1 directs assembly of the HsCyk-4 RhoGAP/Ect2 RhoGEF complex to initiate cleavage furrow formation. PLoS Biol 7, e1000110.
Zhao WM, Fang G (2005). Anillin is a substrate of anaphase-promoting complex/cyclosome (APC/C) that controls spatial contractility of myosin during late cytokinesis. J Biol Chem 280, 33516–33524.
Zonies S, Motegi F, Hao Y, Seydoux G (2010). Symmetry breaking and polarization of the *C. elegans* zygote by the polarity protein PAR-2. Development 137, 1669–1677.